Cellular/Molecular

Localized Calcineurin Confers Ca^{2+}-Dependent Inactivation on Neuronal L-Type Ca^{2+} Channels

Seth F. Oliveria,[1,2,3] Philip J. Dittmer,[1] Dong-ho Youn,[1,4] Mark L. Dell'Acqua,[1,2] and William A. Sather[1,2]

[1]Department of Pharmacology, [2]Program in Neuroscience, and [3]Medical Scientist Training Program, University of Colorado School of Medicine, Aurora, Colorado 80045, and [4]Department of Oral Physiology, School of Dentistry, Kyungpook National University, Daegu 700-412, Korea

Excitation-driven entry of Ca^{2+} through L-type voltage-gated Ca^{2+} channels controls gene expression in neurons and a variety of fundamental activities in other kinds of excitable cells. The probability of opening of $Ca_V1.2$ L-type channels is subject to pronounced enhancement by cAMP-dependent protein kinase (PKA), which is scaffolded to $Ca_V1.2$ channels by A-kinase anchoring proteins (AKAPs). $Ca_V1.2$ channels also undergo negative autoregulation via Ca^{2+}-dependent inactivation (CDI), which strongly limits Ca^{2+} entry. An abundance of evidence indicates that CDI relies upon binding of Ca^{2+}/calmodulin (CaM) to an isoleucine–glutamine motif in the carboxy tail of $Ca_V1.2$ L-type channels, a molecular mechanism seemingly unrelated to phosphorylation-mediated channel enhancement. But our work reveals, in cultured hippocampal neurons and a heterologous expression system, that the Ca^{2+}/CaM-activated phosphatase calcineurin (CaN) is scaffolded to $Ca_V1.2$ channels by the neuronal anchoring protein AKAP79/150, and that overexpression of an AKAP79/150 mutant incapable of binding CaN (ΔPIX; CaN-binding PXIXIT motif deleted) impedes CDI. Interventions that suppress CaN activity—mutation in its catalytic site, antagonism with cyclosporine A or FK506, or intracellular perfusion with a peptide mimicking the sequence of the phosphatase's autoinhibitory domain—interfere with normal CDI. In cultured hippocampal neurons from a ΔPIX knock-in mouse, CDI is absent. Results of experiments with the adenylyl cyclase stimulator forskolin and with the PKA inhibitor PKI suggest that Ca^{2+}/CaM-activated CaN promotes CDI by reversing channel enhancement effectuated by kinases such as PKA. Hence, our investigation of AKAP79/150-anchored CaN reconciles the CaM-based model of CDI with an earlier, seemingly contradictory model based on dephosphorylation signaling.

Introduction

Voltage-gated Ca^{2+} channel activity is tuned to cellular need by a variety of processes, with Ca^{2+}-dependent inactivation (CDI) providing one form of Ca^{2+}-driven feedback control. Elimination of CDI from L-type $Ca_V1.2$ channels pathologically prolongs action potentials in cardiomyocytes (Alseikhan et al., 2002), illustrating the importance of feedback regulation of Ca^{2+} channels. CDI also reduces non-L-type $Ca_V2.1$ channel activity and thereby contributes to short-term synaptic depression during repetitive stimulation (Mochida et al., 2008).

The Ca^{2+} sensor for CDI is Ca^{2+}/calmodulin (CaM) (Peterson et al., 1999; Zühlke et al., 1999), which at resting $[Ca^{2+}]_{in}$ is preassociated with the $Ca_V1.2$ C terminus (Pitt et al., 2001; Erickson et al., 2001, 2003). Ca^{2+} entering the cytoplasm through $Ca_V1.2$ binds to CaM, initiating Ca^{2+}/CaM interaction with an isoleucine–glutamine (IQ) motif located adjacent to the CaM preassociation site (Zühlke et al., 1999, 2000; Erickson et al., 2003; Kim et al., 2004). Because disruption of the IQ motif impairs CDI, Ca^{2+}/CaM interaction with the IQ motif has been proposed to induce directly a change in channel conformational that corresponds to CDI.

But two sets of observations suggest an alternative to this nonenzymatic model of CDI. First, $Ca_V1.2$-anchored Ca^{2+}/CaM often acts via downstream enzymes. Examples include Ca^{2+}-dependent facilitation (CDF) of $Ca_V1.2$ by CaM-dependent protein kinase II (CaMKII) (Noble and Shimoni, 1981; Zühlke et al., 2000; Hudmon et al., 2005; Erxleben et al., 2006; Grueter et al., 2006) and coupling of neuronal excitation to activation of transcription factors by kinases and phosphatases (Dolmetsch et al., 2001; Oliveria et al., 2007). Second, Chad and Eckert (1986) found for molluscan neurons that protein kinase A (PKA) activity slowed Ca_V channel inactivation, and that calcineurin (CaN) opposed this effect, suggesting an enzymatic mechanism for CDI (for review, see Armstrong, 1989). Modulation by PKA of $Ca_V1.2$ CDI has since been described in a variety of excitable cell types (Bean et al., 1984; Kalman et al., 1988; Hadley and Lederer, 1991; Meuth et al., 2002). Yet a role for CaN in CDI has remained controversial, in part owing to inconsistent responses to inhibition of CaN (Branchaw et al., 1997; Victor et al., 1997; Lukyanetz et al., 1998; Burley and Sihra, 2000; Zeilhofer et al., 2000; Meuth et al., 2002) and to a lack of appreciation of the role of scaffolding proteins in targeting CaN to $Ca_V1.2$.

In hippocampal neurons, Ca^{2+} and cAMP reciprocally regulate L channel activity by activation of CaN and PKA that are coanchored to $Ca_V1.2$ channels by the scaffolding protein AKAP79/150 (human/rodent) (Oliveria et al., 2007). AKAP79/150-anchored CaN suppresses enhancement of neuronal L-type Ca^{2+} channel activity by coanchored, activated PKA (Oliveria et

Received May 12, 2012; revised Aug. 15, 2012; accepted Aug. 29, 2012.

Author contributions: S.F.O., M.L.D., and W.A.S. designed research; S.F.O., P.J.D., and D.-h.Y. performed research; S.F.O., P.J.D., D.-h.Y., M.L.D., and W.A.S. analyzed data; S.F.O., P.J.D., D.-h.Y., M.L.D., and W.A.S. wrote the paper.

This work was supported by NIH Grants F30-NS051963, T32-AA007464, R01-MH080291, and R01-HL088548.

The authors declare no competing financial interest.

Correspondence should be addressed to William A. Sather, University of Colorado School of Medicine, Mail Stop 8315, 12800 East 19th Avenue, Aurora, CO 80045. E-mail: william.sather@ucdenver.edu.

S. Oliveria's present address: Department of Neurosurgery, University of Florida, Gainesville, FL 32610.

DOI:10.1523/JNEUROSCI.2302-12.2012

 0270-6474/12/3215328-10$15.00/0

al., 2007). CaN effectiveness can in part be attributed to its localization within the $Ca_V1.2$ macromolecular complex, where CaN is advantageously placed to interact with its activator, Ca^{2+}/CaM. Here we describe experimental results indicating that CaM, the Ca^{2+} sensor for CDI, triggers CDI in hippocampal neurons by activating AKAP879/150-anchored CaN.

Materials and Methods

Cell culture and transfection of tsA201 cells. tsA201 cells were transfected with equimolar ratios of cDNAs encoding $Ca_V1.2$ channel subunits ($\alpha_1$1.2a, β_{2b}, $\alpha_2\delta_{1a}$) and other proteins, including AKAP79, using the Effectene transfection reagent (Qiagen). Cells were plated onto glass coverslips and studied 1–3 d after transfection.

Preparation and transfection of primary, short-term cultured hippocampal neurons. Primary hippocampal neurons were prepared from neonatal Sprague Dawley rats [postnatal day 0 (P0)–P3] as described previously (Gomez et al., 2002; Smith et al., 2006). For Amaxa Nucleofector transfection, P0–P3 neurons were resuspended at 2×10^6 to 3×10^6 cells per transfection, electroporated with 6–8 μg of total DNA (including GFP or CaN_{H151A}-YFP cDNA and/or the 150RNAi construct), plated at 0.25×10^6 to 0.5×10^6 cells per 25 mm glass coverslip, and grown up to 6 d *in vitro*. Current waveform and tail current time course indicated that these short-term cultured neurons were electrotonically more compact than older neurons, permitting analysis of the inactivation kinetics of pharmacologically isolated L currents.

AKAP150ΔPIX *knock-in mice. AKAP150ΔPIX* mice were developed in conjunction with the Rocky Mountain Neurological Disorders Transgenic and Gene Targeting Vectors Core and housed at the University of Colorado Anschutz Medical Campus Center for Comparative Medicine. Briefly, the *AKAP150ΔPIX* mutation, which removes the conserved PIAIIIT motif (amino acids 655–661), was introduced into the single AKAP150 coding exon in the AKAP5 gene by homologous recombination in C57BL/6J×129 F1 embryonic stem cells using a loxP-flanked neomycin cassette located downstream of the exon. Targeted ES clones were identified by G418 selection for the neomycin resistance gene and PCR screening of genomic DNA, expanded, and injected into blastocysts that were implanted into surrogate females. Heterozygous and homozygous mice carrying the mutation were derived from the resulting F0 chimeric founders by standard breeding with C57BL/6J. *AKAP150ΔPIX* mice housed in a home-cage environment had no obvious phenotypic alterations in body weight, life span, breeding, or behavior. A full description of the *AKAP150ΔPIX* knock-in targeting vector and additional details of generation and characterization of *AKAP150ΔPIX* mice was reported by Sanderson et al. (2012). Dissociated mouse neurons were cultured as for rat neurons.

Patch-clamp recording. Borosilicate patch pipettes were heat-polished to a resistance, measured in the bath, of 3–6 MΩ. Voltage-clamped currents were measured with an Axopatch 1D amplifier (Molecular Devices), filtered at 2 kHz, and sampled at 10 kHz using Pulse software (HEKA) and an ITC-16 analog-to-digital and digital-to-analog interface (HEKA). Series resistance compensation, capacitance cancellation, and leak subtraction (−P/4 protocol) were used.

For tsA201 cells, the whole-cell pipette contained the following (in mM): 135 CsCl, 10 EGTA or 1,2-bis(*o*-aminophenoxy)ethane-*N*,*N*,*N*′,*N*′-tetraacetic acid (BAPTA), 10 HEPES, and 4 MgATP, pH adjusted to 7.5 with tetraethylammonium-hydroxide (TEA-OH). For recordings in Ca^{2+} or Ba^{2+}, the bath solution contained the following (in mM): 125 NaCl, 15 $CaCl_2$ or 15 $BaCl_2$, 10 HEPES, and 20 sucrose, pH adjusted to 7.3 with TEA-OH. For recordings of Na^+ currents carried by Ca^{2+} channels, the whole-cell pipette contained the solution described above, but supplemented with 10 mM BAPTA, and the bath solution contained the following (in mM): 140 NaCl, 5 CsCl, 5 EGTA, 10 HEPES, and 20 sucrose, pH adjusted to 7.3 with TEA-OH. Positive transfectants were identified by GFP, AKAP79-YFP, CaM-YFP, CaN-CFP, or CaN-YFP fluorescence. When unlabeled AKAP79 was transfected, only cells exhibiting membrane-localized CaN were selected for recording. In each tsA201 cell where inactivation rate was studied, the holding potential was −80 mV, and a sequence of 500-ms step depolarizations, from −60 to +70 mV in 10 mV increments, was applied for both Ca^{2+} and Ba^{2+} solutions. A fast perfusion system (Warner Instruments) and slower bath perfusion were used in combination to ensure rapid and complete solution exchange. Cells that exhibited an artifactual current–voltage relationship were excluded from further analysis. $CdCl_2$ (200 μM) was applied at the end of each experiment to isolate Ca^{2+} current and Ba^{2+} current from leak or other contamination. Na^+ current recordings were performed similarly, but not in the same cells as the Ca^{2+} and Ba^{2+} current recordings. To provide a reliable basis for comparison of Ca^{2+} and Ba^{2+} inactivation rates, currents were generally allowed to stabilize for ~5 min after establishment of whole-cell recording. In the experiments examining the time course of development for forskolin action inactivation (see Fig. 5), the stabilization period was necessarily omitted.

For cultured hippocampal pyramidal neurons, the whole-cell pipette contained the following (in mM): 120 $CsMeSO_4$, 30 TEA-Cl, 10 EGTA, 5 $MgCl_2$, 5 Na_2ATP, and 10 HEPES, pH 7.2. The extracellular solution contained the following (in mM): 125 NaCl, 10 $BaCl_2$ or $CaCl_2$, 5.85 KCl, 22.5 TEA-Cl, 1.2 $MgCl_2$, 10 HEPES(Na), and 11 D-glucose, pH 7.4, as well as tetrodotoxin (1 μM). To isolate L-type currents, N- and P/Q-type Ca^{2+} channel currents were blocked by preincubating neurons in extracellular recording solution supplemented with ω-conotoxins (ω-CTx) GVIA (1 μM) and MVIIC (5 μM) for 30 min before recording (Tavalin et al., 2004; Oliveria et al., 2007). Neurons were used for <1 h after preincubation to minimize contamination from unblocked N- and P/Q-type currents [τ_{off}, ~200 min for ω-CTx-MVIIC unbinding from P/Q-type channels (Sather et al., 1993); ω-CTx-GVIA binding to N-type channels was even more prolonged (McCleskey et al., 1987)]. A holding potential of −60 mV was chosen to inactivate R-type Ca^{2+} channel current (>80%) (Sochivko et al., 2003). Transfected neurons were identified by GFP or CaN_{H151A}-YFP fluorescence. Only neurons with an access resistance <10 MΩ were studied.

To analyze inactivation time course during 500 ms depolarizations to 0 mV, the decaying phase of each current record was best fit with a double-exponential function; in a very few cases, single exponential fits provided, by eye, equally good fits (PulseFit software; HEKA). For the double-exponential fits, the faster time constant (τ_{fast}) provided an index of Ca^{2+}-dependent inactivation, and the slower component represented voltage-dependent inactivation (Adams and Tanabe, 1997). Currents were obtained in Ba^{2+} and Ca^{2+} in the same cell, with Ba^{2+} currents recorded before Ca^{2+} currents.

Where indicated, forskolin (5 μM), protein kinase inhibitor fragment (PKI; residues 6–22; 5 μM), cyclosporin A (CsA; 5 μM), the CaN autoinhibitory peptide (AIP; residues 457–482; 100 μM), or CaN anchoring antagonist peptide VIVIT (Oliveria et al., 2007; Li et al., 2012) (biotin-GPHPVIVITGPHEE, 10, 25 or 100 μM) was included in the pipette solution. To examine reversibility of CaN inhibition, cyclosporin and FK506 (10 μM each) were added to the bath in some experiments, as indicated in the text. Forskolin, PKI, cyclosporin A, and FK506 were obtained from Sigma-Aldrich; the CaN autoinhibitory peptide was obtained from Biomol; and the VIVIT peptide was obtained from Biomatik.

Ratiometric fluorometry. Measurements of YFP^{535}/CFP^{470} were made using a ratiometric fluorimeter (Solamere Technology Group) where the donor fluorophore, CFP, was excited (excitation bandpass, 436 ± 5 nm), and emissions from both CFP (CFP^{470}) and YFP (YFP^{535}) were collected using parallel photomultiplier tubes fronted by a dichroic mirror and bandpass filters (CFP bandpass, 470 ± 15 nm; YFP bandpass, 535 ± 15 nm). In all experiments, simultaneous emission ratio (YFP^{535}/CFP^{470}) and current (I_{Ca}) measurements were obtained. CFP was excited (shutter open) for 50 ms periods centered in time on the membrane depolarizations (20 ms steps; 0.067 or 1 Hz), and the emission ratio was measured as the mean YFP^{535}/CFP^{470} value during each 50 ms depolarization. Concurrent I_{Ca} and YFP^{535}/CFP^{470} signals were acquired and recorded using Pulse software (HEKA). The step depolarization frequency of 0.067 Hz was chosen to establish baseline emission ratio and current values because this was the highest frequency that was indistinguishable from the

baseline determined for cells held at −80 mV for an extended period between depolarizing steps.

Fluorescence resonance energy transfer microscopy. Fluorescence images were acquired 2–3 d after transfection from live tsA201 cells using a Nikon TE-300 inverted microscope equipped with a 175 W xenon illumination source, 100× oil-immersion objective lens, 16 MHz CCD camera (SensiCam QE; Cooke), and dual filter wheels (Sutter Instruments) controlled by SlideBook 4.0 software (Intelligent Imaging Innovation). For sensitized fluorescence resonance energy transfer (FRET) measurements [$FRET^C$; three filter (3F)], an 86002 (JP4) dichroic mirror (Chroma) and three different filter sets (donor/CFP, acceptor/YFP, and raw FRET) were used to capture serially a set of three images from a fixed image plane. The three images were captured using the same exposure time (100 ms in some experiments, 250 ms in others). The three filter sets used were donor [*CFP*; 436 center excitation wavelength and 10 nm bandwidth (436/10 nm); emission, 470/30 nm], acceptor (*YFP*; excitation, 500/20 nm; emission, 535/30 nm), and FRET (*raw FRET*; excitation, 436/10 nm; emission, 535/30 nm). Light that has passed through the FRET filter set is contaminated by donor bleed-through (average fraction, 0.50) and acceptor cross-excitation (average fraction, 0.02); fractional contamination by bleed-through and cross-excitation were determined in separate experiments using cells that expressed CFP- or YFP-tagged constructs alone. Corrected, sensitized FRET ($FRET^C$) images were obtained by subtracting the contamination components, pixel by pixel, from raw FRET images using the following equation (adapted from Gordon et al., 1998): $FRET^C = raw\text{-}FRET - (0.50 * CFP) - (0.02 * YFP)$.

To obtain estimates of effective FRET efficiency (E_{eff}) from images, Slidebook 4.0 was used to draw masks that isolated in-focus CaN-CFP fluorescence. From masked raw FRET, CFP, and YFP images, the FRET ratio (*FR*) was extracted as $FR = [rawFRET - (0.5 * CFP)]/(0.02 * YFP)$.

E_{eff} was then calculated as $E_{eff,\,3F} = (FR - 1) * (\varepsilon_{YFP440}/\varepsilon_{CFP440})$, where ε_{YFP440} and ε_{CFP440} represent the average molar extinction coefficients for YFP and CFP over the bandpass of the CFP excitation filter, respectively. The measurement E_{eff} takes into account cell-to-cell variation in expression of YFP and CFP, so that this FRET index is effectively independent of donor and acceptor concentration (Erickson et al., 2003; Oliveria et al., 2007).

FRET was additionally estimated using an acceptor photobleach (PB) method. PB measurements were obtained from the same cells used to make the 3F measurements. PB FRET was measured as the difference between CFP (donor) fluorescence intensity before and after photobleach of YFP (acceptor). Photobleach was achieved by several minutes of continuous illumination at 535 nm, and was virtually complete. E_{eff} was calculated from acceptor photobleach images as $E_{eff,\,PB} = 1 - (F_{DA}/F_D)$, where F_{DA} and F_D indicate donor intensity before and after photobleaching, respectively [E_{eff} calculations are adapted from the study by Erickson et al. (2003)].

Statistical analysis. Statistical analyses were performed using Student's *t* test, ANOVA, or Bonferroni's test. All error bars indicate SEM.

Results

AKAP79 and the $Ca_V1.2$ IQ motif sustain CaM–CaN signaling

We showed previously that $Ca_V1.2$ currents enhanced by the adenylyl cyclase agonist forskolin can be de-enhanced through CaN activation during episodes of increased stimulation frequency (Oliveria et al., 2007). To test whether CaM docked at the IQ motif is the activator of anchored CaN, we recorded forskolin-enhanced $Ca_V1.2$ currents from tsA201 cells while monitoring CaM–CaN interaction in response to an increase in step-depolarization frequency from 0.067 to 1 Hz. CaM stimulation of CaN was monitored by the CaM-YFP^{535}/CaN-CFP^{470} fluorescence emission ratio in response to CFP^{436} excitation, which provides a FRET-based readout of changes in CaM–CaN interaction. Increasing depolarization frequency in voltage-clamped, transfected tsA201 cells caused a rapid increase in CaM-YFP^{535}/CaN-CFP^{470}, which appeared to proceed as fast as, or slightly faster than, de-enhancement of current (Fig. 1*A*). When intracellular EGTA was replaced with BAPTA, neither the change in YFP^{535}/CFP^{470} ratio nor de-enhancement was observed upon increase in depolarization frequency (Fig. 1*B*). Differential sensitivity to BAPTA versus EGTA indicates that the change in YFP^{535}/CFP^{470} occurs in response to increased $[Ca^{2+}]$ in the channel's nanoenvironment. These findings, along with previous ones showing that de-enhancement was fully prevented by intracellular dialysis with a peptide that mimics the CaN autoinhibitory domain and blocks CaN (Oliveria et al., 2007), together suggest that in our system Ca^{2+}/CaM activates CaN, which in turn acts to de-enhance activity of $Ca_V1.2$ channels.

Unlike the strong CaN activation signal we observed in cells expressing $Ca_V1.2$ channels with wild-type AKAP79, CaN activation was defective when the AKAP79–CaN interaction was disrupted via deletion of the CaN-binding AKAP79 PxIxIT-like motif (79ΔPIX). In cells expressing 79ΔPIX, the extent of apparent CaM–CaN interaction declined subsequent to the increase in depolarization frequency (Fig. 1*C*), revealing a detectable amount of CaM–CaN association even when the channel was only activated at low frequency. Currents recorded from channels lacking scaffolded CaN retained a residual degree of de-enhancement, as though they were weakly regulated by the phosphatase even in the absence of AKAP79 anchoring.

When the $Ca_V1.2$ IQ motif-CaM interaction was disrupted by the well-characterized IQ-to-EQ mutation (IQ/EQ) (Zühlke et al., 1999; Erickson et al., 2003; Kim et al., 2004), the strength of the CaM–CaN interaction signal also declined as depolarization frequency was increased (Fig. 1*D*). As for cells expressing 79ΔPIX, this decline reveals detectable CaM–CaN association near $Ca_V1.2_{IQ/EQ}$ channels during low-frequency channel activation. Intriguingly, for channels containing the IQ/EQ mutation, increased stimulation frequency relieved channel inhibition that was present during the preceding period of low-frequency channel activity, as seen by a transient increase in current amplitude. The effects of the IQ/EQ and 79ΔPIX mutations indicate that IQ–CaM and AKAP79–CaN interactions are both necessary to sustain effective CaN-mediated opposition to PKA enhancement of channel activity.

CaM and CaN preassemble near $Ca_V1.2$ at resting Ca^{2+}

Because CaN was able to partially suppress $Ca_V1.2$ activity during high-frequency depolarization in 79ΔPIX cells (Fig. 1*C*), we tested whether CaM and CaN are able to associate near the channel independent of AKAP79. To do this, we imaged FRET between CaM-YFP and CaN-CFP using two independent methods of measuring effective FRET efficiency: 3F and PB. When CaM-YFP and CaN-CFP were coexpressed with channel subunits and AKAP79, we observed FRET between CaM and CaN in live cells that was strongest near the plasma membrane (Fig. 1*E*,*F*). In contrast, FRET was absent when the pore-forming $Ca_V1.2$ channel subunit was not expressed or when cells were loaded with BAPTA-AM. Since the $Ca_V1.2$ C terminus contains both the IQ motif and a modified leucine zipper motif that helps support $Ca_V1.2$–AKAP79 interaction, one possible explanation for these observations is that the channel C terminus promotes CaM–CaN FRET between IQ-docked CaM and AKAP79-scaffolded CaN. However, CaN–CaM FRET persisted when FRET measurements were performed in cells expressing either $Ca_V1.2_{IQ/EQ}$ or 79ΔPIX (Fig. 1*G*), indicating that in tsA201 cells, neither the CaN-binding site on AKAP79 nor the IQ motif is necessary for CaM–CaN preassemble within the $Ca_V1.2$ complex at resting $[Ca^{2+}]_{in}$.

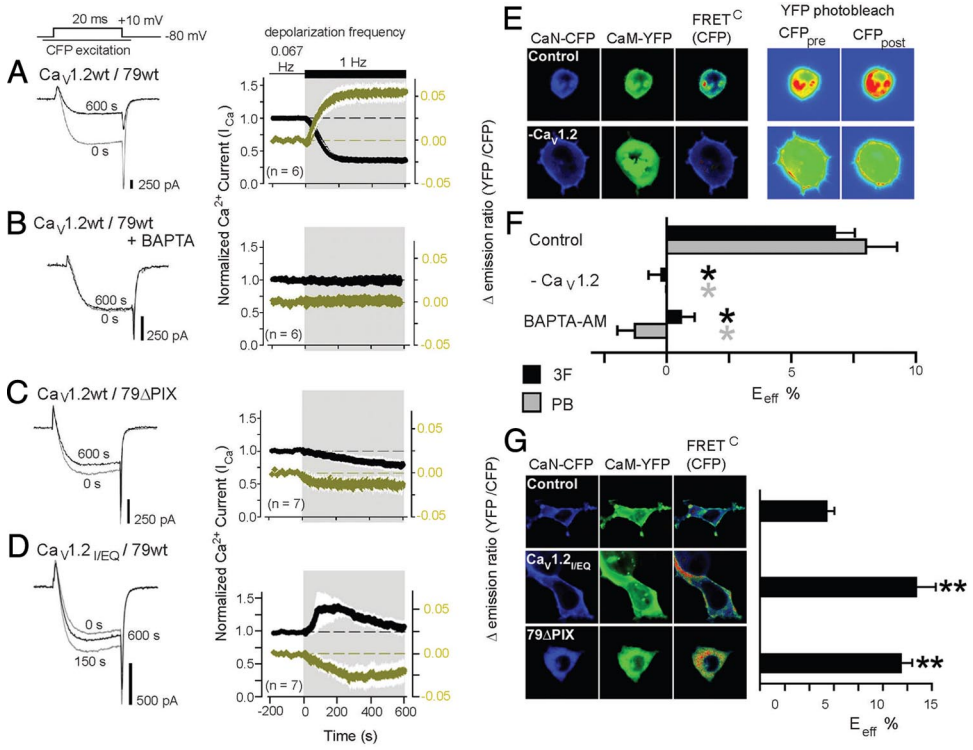

Figure 1. In transfected tsA201 cells, AKAP79 and the IQ motif in $Ca_V1.2$ sustain CaM–CaN signaling during heightened channel activity. ***A–D***, After establishing a steady baseline for both forskolin-enhanced $Ca_V1.2$ Ca^{2+} current amplitude (I_{Ca}) and YFP^{535}/CFP^{470} emission ratio in response to step depolarization once every 15 s (0.067 Hz), depolarization frequency was increased to 1 Hz. Cells expressing channel subunits, AKAP79, CaN-CFP, and CaM-YFP (***A***), internally perfused with 10 mM intracellular BAPTA in place of 10 mM EGTA (***B***), expressing AKAP79PIX (79ΔPIX) in place of AKAP79 (***C***), and expressing $Ca_V1.2_{IQ/EQ}$ in place of wild-type $Ca_V1.2$ (***D***) are shown. Left, Ca^{2+} current records evoked before (0 s) and after 600 s of 1 Hz depolarizations. Right, Time course of response to increased depolarization frequency for both Ca^{2+} current (black) and YFP^{535}/CFP^{470} (gold). Ca^{2+} current was normalized to the value obtained at 0 s; when necessary, time courses were corrected for the rate of channel rundown at 0.067 Hz. ΔYFP^{535}/CFP^{470} indicates the change in the emission ratio relative to the average value at 0.067 Hz. The white envelope against the shaded background represents SEM. ***E***, Left, Micrographs showing subcellular localization of CaN-CFP, CaM-YFP, and corrected, sensitized FRET gated to donor intensity [*FRET^C (CFP)*; pseudocolor]. Right, Pseudocolor images representing FRET donor intensity before (*CFP$_{pre}$*) and after (*CFP$_{post}$*) acceptor photobleaching. ***F***, Effective FRET efficiency calculated from both 3F and also YFP-acceptor PB measurements in some conditions. $Ca_V1.2$, β_{2b}, $\alpha_2\delta$, and AKAP79 were coexpressed with fluorescent CaN-CFP and CaM-YFP, except when $Ca_V1.2$ was omitted ($-Ca_V1.2$). In the BAPTA-AM experiments, cells were bathed in 100 μM BAPTA-AM for 60 min. $n > 10$ for all conditions. *$p < 0.001$ (black) vs 3F control; *$p < 0.001$ (gray) vs PB control (by both ANOVA and Bonferroni's test). ***G***, Left, Micrographs showing subcellular localization of CaN-CFP, CaM-YFP, and corrected, sensitized FRET gated to donor intensity [*FRET^C (CFP)*; pseudocolor] in cells coexpressing unlabeled $Ca_V1.2$, β_{2b}, $\alpha_2\delta$, and AKAP79. $Ca_V1.2_{IQ/EQ}$ and 79ΔPIX were expressed in place of wild-type $Ca_V1.2$ and AKAP79 as indicated. Right, Three-filter-set effective FRET efficiency. $n > 10$ for all conditions. **$p < 0.001$ vs control (by both ANOVA and Bonferroni's test).

Calcineurin phosphatase activity triggers CDI of $Ca_V1.2$ channels

Given these results and the established role of CaM binding to the IQ motif in $Ca_V1.2$ CDI, we revisited the possibility that CaN might contribute to CDI. During 500-ms-step depolarization, AKAP79-associated $Ca_V1.2$ channels exhibited strong ion-dependent inactivation (measured as $1/\tau_{fast}$) with Ca^{2+} as the current carrier, but much less inactivation when current was carried by Ba^{2+} (Fig. 2*A*). CDI was most evident when Ca^{2+} influx was greatest (Brehm and Eckert, 1978; Lee et al., 1985): depolarization that evoked smaller Ca^{2+} current elicited little CDI, while depolarization that evoked maximal Ca^{2+} current (peak of the current–voltage relationship) elicited maximum CDI.

CDI was significantly slowed when a catalytically inactive mutant of CaN (CaN_{H151A}) (Mondragon et al., 1997) was transfected along with AKAP79 and the $Ca_V1.2$ subunits. Suppression of AKAP79 expression by a well-characterized RNAi construct (Hoshi et al., 2005) also slowed CDI, but this was less effective than CaN_{H151A} (Fig. 2*B*). Combining CaN_{H151A} overexpression with RNAi suppression of AKAP79, thus disrupting both CaN activity and anchoring, prevented CDI (Fig. 2*B*). These results suggest that when it could be scaffolded to channels by AKAP79, endogenous CaN remained partially effective in regulating channel activity despite competing against overexpressed CaN_{H151A}. CDI was also reduced by an alternative means of inhibiting CaN: in cells transfected with AKAP79 and $Ca_V1.2$ subunits, intracellular perfusion with the CaN autoinhibitory peptide significantly depressed CDI (Fig. 2*C*). CDI was suppressed, albeit incompletely, by the Ca^{2+} chelator BAPTA (Fig. 2*C*), indicating that Ca^{2+} entry activates CDI and that the Ca^{2+} sensor that initiates CDI must be located close to the point of Ca^{2+} entry. Comparison of the full suppression by BAPTA of CaN-mediated channel de-enhancement during high-frequency stimulation (Fig. 1*D*) with the partial slowing of CDI during 500 ms depolarizations (Fig. 2*C*, middle) suggests that these two means of measuring CDI reveal different aspects of a single underlying mechanism. In either case, our results indicate that AKAP-anchored CaN, like IQ-bound Ca^{2+}/CaM, signals within the channel nanodomain.

Ba^{2+} is a weak agonist for CDI

Inactivation of Ba^{2+} current carried by $Ca_V1.2$ is typically taken to represent voltage-dependent inactivation. But compared to inactivation of Ba^{2+} currents, Na^+ currents through $Ca_V1.2$ channels exhibited much slower inactivation rates across the entire range of depolarizing pulses that evoked inward current (Fig. 3). Hence, it seems likely that Ba^{2+} acts as a weak agonist for CDI.

This idea is supported by the observation that CaN_{H151A} slowed inactivation of Ba^{2+} current (Fig. 2*A*,*B*) but not of Na^+ current (Fig. 3*A*).

AKAP79-targeted PKA modulates CDI

AKAP79/150-anchored PKA and CaN act as opponents in regulating L channel opening (Oliveria et al., 2007), predicting that active PKA might counter CaN-dependent CDI. Forskolin stimulation of PKA did not affect $Ca_V1.2$ inactivation (Fig. 4), perhaps because AKAP79 coanchoring of CaN allows the catalytically faster phosphatase to overcome PKA activity in the nanoenvironment of each channel (Oliveria et al., 2007). At a basal level of PKA activity, CDI was slightly slowed by expression of the CaN-anchoring-defective 79ΔPIX mutant, but stimulating PKA activity with forskolin in cells expressing 79ΔPIX slowed Ca^{2+} current inactivation nearly to the rate for Ba^{2+} (Fig. 4). Therefore it seems that in the presence of anchored and active PKA, CaN requires AKAP79/150 to overcome current enhancement by PKA and effectuate CDI. If CDI does indeed represent reversal of PKA phosphorylation of the channel by CaN, then CDI should also be sensitive to disruption of PKA enhancement. In accord with this idea, CDI was significantly slower when PKA activity was inhibited with PKI. However, inhibition of PKA did not eliminate CDI, as though PKA was not solely responsible for phosphorylation of the channel complex.

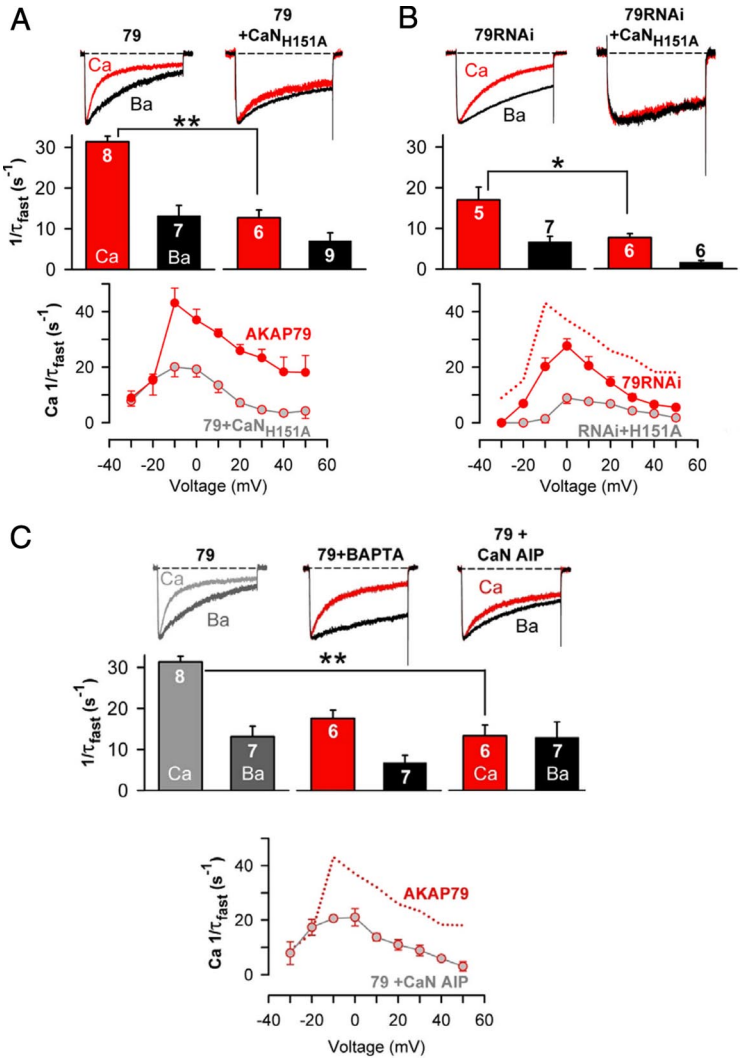

Figure 2. Localized calcineurin phosphatase activity triggers CDI of $Ca_V1.2$ channels heterologously expressed in tsA201 cells. ***A***, Top, Ca^{2+} (red) and Ba^{2+} (black) currents recorded from the same cell by a 500 ms depolarization from −80 to +10 mV. Ca^{2+} and Ba^{2+} currents are shown scaled to the same peak inward current amplitude to facilitate comparison of inactivation rate. In addition to the three channel subunits, AKAP79 was overexpressed either alone (79) or with CaN_{H151A}. Middle, Inactivation rates for Ca^{2+} current (red bars) and Ba^{2+} current (black bars). Number of individual cells recorded (*n*) is marked on the bars. Bottom, Ca^{2+} current inactivation rates over the range of test potentials that elicited inward current in cells overexpressing AKAP79 alone or AKAP79 + CaN_{H151A}. $^{**}p < 0.001$ (Student's *t* test). ***B***, As in ***A***, except that endogenous AKAP79 was suppressed (79RNAi), either alone or in combination with CaN_{H151A} overexpression. $^{*}p < 0.05$ (Student's *t* test). ***C***, $Ca_V1.2$ Ca^{2+} (red) and Ba^{2+} (black) current records and inactivation rates with 10 mM intracellular BAPTA in place of 10 mM EGTA, or with the CaN AIP (100 μM) perfused into the cell via the patch pipette. Data for AKAP79-overexpressing cells, shown in gray, are reproduced from ***A*** for comparison. $^{**}p < 0.001$ (ANOVA and Bonferroni's test). Rates of inactivation of Ca^{2+} current over the range of test potentials that elicited inward current in AKAP79-expressing cells that were exposed to the CaN AIP. Dotted red line reproduces from ***A*** the voltage dependence of Ca^{2+} current inactivation measured from control AKAP79-expressing cells without the CaN AIP. Ca^{2+} current densities were as follows (in pA/pF): 79, −37.1 ± 6.3; 79 + CaN_{H151A}, −33.8 ± 7.4; 79RNAi, −35.0 ± 13; 79RNAi + CaN_{H151A}, −27.4 ± 6.4; 79 + BAPTA, −31.1 ± 7.1; 79 + CaN AIP, −32.8 ± 8.6. No forskolin was used in the experiments.

AKAP79-anchored calcineurin mediates CDI of $Ca_V1.2$ channels by opposing PKA

As an alternative means of studying PKA opposition to CaN, we studied the dynamics of development of this process in individual cells. Following patch rupture and initiation of whole-cell recording, internal perfusion with forskolin progressively slowed CDI in tsA201 cells transfected with 79ΔPIX, but not in cells transfected with wild-type AKAP79 (Fig. 5*A*). During intracellular perfusion of wild-type AKAP79 cells with forskolin, bath application of the CaN antagonists CsA and FK506, which inhibit CaN through distinct cyclophilin and FKBP pathways, was able to reduce CDI (Fig. 5*B*). The acute effect on CDI of this combination of CsA and FK506 was reversed upon washout. Together, the results support the idea that PKA, stimulated by elevation of cAMP with forskolin, can oppose CaN-mediated inactivation of Ca^{2+} current.

CaN contributes to CDI of L-type Ca^{2+} channels in cultured hippocampal neurons

As powerful as reconstitution in heterologous expression systems is for investigating mechanisms of channel regulation, models ultimately need to be tested in the biological system of interest, in this case, hippocampal neurons. We found previously that AKAP-anchored CaN powerfully regulates L-type Ca^{2+} currents in hippocampal neurons (Oliveria et al., 2007), so we next examined whether CaN might do so via CDI.

Pharmacologically isolated L-type Ca^{2+} current recorded from short-term cultured rat hippocampal neurons show robust CDI characterized by rapid inactivation in Ca^{2+} compared to Ba^{2+}. Consistent with a role for AKAP79/150 in CDI, inactivation was much slower when expression of the rodent ortholog of human AKAP79, AKAP150, was suppressed with a previously characterized RNAi construct (Hoshi et al., 2005;

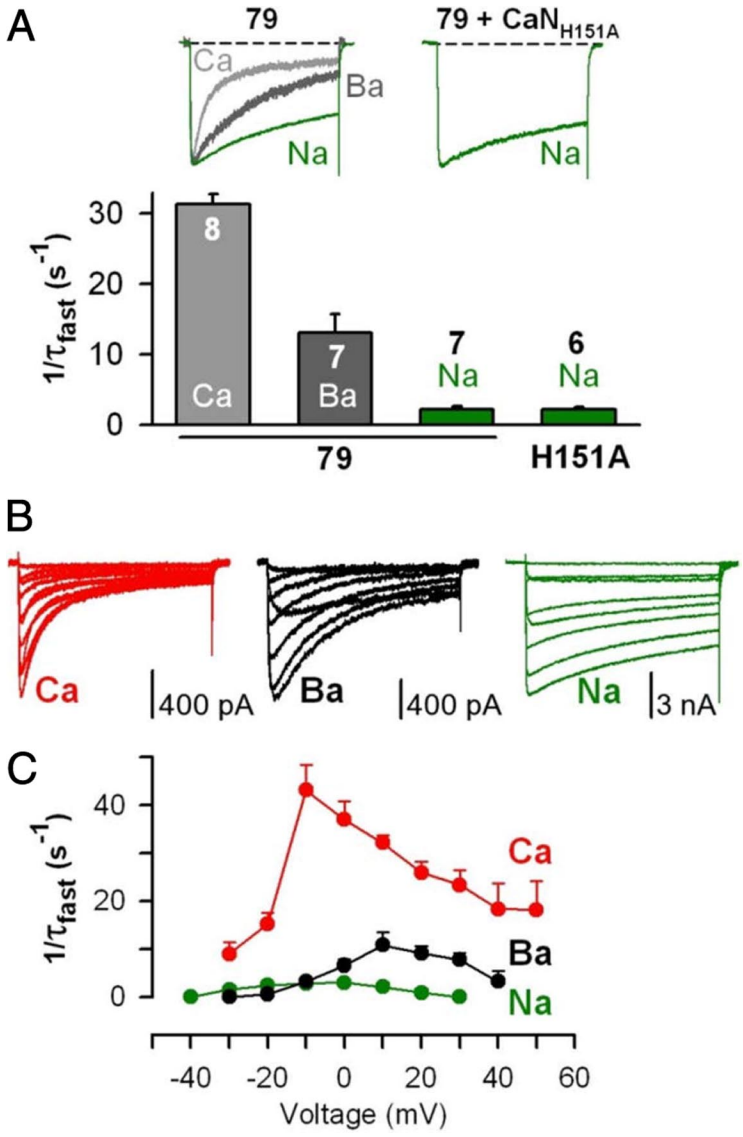

Figure 3. Ba^{2+} acts as a weak agonist for CDI of $Ca_V1.2$ channels in tsA201 cells. ***A***, Top, Recordings of Na^+ current (green) evoked by 500 ms depolarization from −80 to −10 mV in cells in which AKAP79 was overexpressed either alone (79) or with CaN_{H151A}. Control $Ca_V1.2$ Ca^{2+} (light gray) and Ba^{2+} (dark gray) current records reproduced from Figure 2*A*. Ca^{2+}, Ba^{2+}, and Na^+ currents are shown scaled to the same peak inward current amplitude. Bottom, Inactivation rates measured for Ca^{2+} (light gray bar), Ba^{2+} (dark gray bar), and Na^+ (green bars) currents carried by $Ca_V1.2$ channels in cells overexpressing AKAP79 (79) or AKAP79 and CaN_{H151A}. Ca^{2+} and Ba^{2+} data reproduced from Figure 2*A*. ***B***, Families of Ca^{2+}, Ba^{2+}, and Na^+ currents through $Ca_V1.2$ channels, recorded over a range of test potentials that elicited inward current in cells overexpressing AKAP79. ***C***, For Ca^{2+}, Ba^{2+}, and Na^+ currents carried by $Ca_V1.2$ channels, inactivation rates obtained over a range of test potentials applied to cells overexpressing AKAP79. No forskolin was used in the experiments.

Oliveria et al., 2007) (Fig. 6*A*). Suppression of CDI by 150RNAi was fully rescued by coexpression of AKAP79 in rat neurons, but no rescue of CDI was observed in neurons cotransfected with 79ΔPIX (Fig. 6*B*). In addition, the strong CDI observed in wild-type mouse neurons was completely absent in neurons cultured from *150ΔPIX* knock-in mice (Sanderson et al., 2012) (Fig. 6*C*).

To confirm a requirement for AKAP-anchored CaN in neuronal CDI, we used an acute means to antagonize CaN anchoring. Internal perfusion with a peptide that mimics the AKAP150 anchoring sequence for CaN, VIVIT (Oliveria et al., 2007; Li et al., 2012), competitively and dose-dependently suppressed CDI of Ca^{2+} current, leaving Ba^{2+} current unaltered (Fig. 7*A*). At the highest concentration tested (100 μM in the whole-cell pipette), VIVIT reduced the rate of inactivation in Ca^{2+} to that measured for Ba^{2+} current. To establish a requirement for CaN phosphatase activity in CDI of neuronal L channels, we used two different approaches: transfection of cultured neurons with CaN_{H151A} and internal perfusion with CsA. Both experimental manipulations strongly reduced the rate of inactivation of Ca^{2+} current carried by neuronal L channels (Fig. 7*B*).

Discussion

In neurons and a heterologous expression system that incorporates the important neuronal scaffolding molecule AKAP79/150, we found that Ca^{2+}/CaM induces CDI of L channels through activation of CaN. A role for CaN in CDI is supported by our observations of significantly slowed inactivation by (1) overexpression of catalytically inactive CaN (CaN_{H151A}), (2) internal dialysis with the CaN autoinhibitory peptide, and (3) application of the CaN antagonist CsA. The fact that CaN_{H151A} had no effect on inactivation of $Ca_V1.2$ Na^+ current indicates that this CaN mutant acts selectively to depress CDI. Expression of L channel CDI in neurons requires anchoring of CaN by AKAP79/150, whereas in the tsA201 expression system, CaN anchoring by AKAP79/150 is not absolutely required but is needed to support rapid, fully developed CDI. Evidence implicating CaN-anchoring by AKAP79/150 in CDI includes (1) elimination of CDI by 150RNAi knockdown and also by replacement with CaN-binding-defective AKAP79ΔPIX, (2) elimination of CDI in a *150ΔPIX* knock-in mouse, and (3) competitive inhibition of CaN anchoring by VIVIT. Overall, interventions that impaired CaN action had more complete effects in neurons than in tsA201 cells, possibly reflecting more natural spatial organization and signaling stoichiometry, or yet-to-be identified regulatory factors.

Dephosphorylation signaling in CDI: permissive and direct models

Although Ca^{2+}/CaM activation of CaN phosphatase activity appears to be a required step for CDI of L channels in hippocampal pyramidal neurons, our results do not exclude the possibility that conformational change of CaM docked to $Ca_V1.2$ can directly inactivate channel activity in some cellular contexts. An extensive body of work has highlighted the centrality of Ca^{2+}/CaM in CDI (for review, see Calin-Jageman and Lee, 2008), but none of this work has taken into consideration the L channel scaffolding protein AKAP79/150, the absence of which minimizes CaN action on L channels. The logic underlying the two different experimental measures of CDI used here—cumulative inactivation during high-frequency depolarization reported by progressive reduction in Ca^{2+} current amplitude versus rate of inactivation during 500 ms depolarization—suggests a pair of

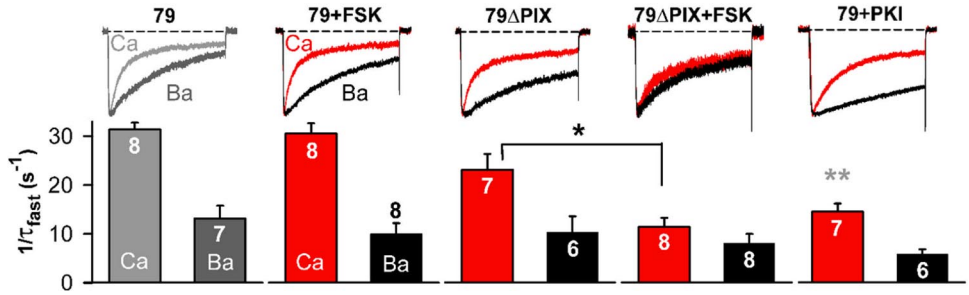

Figure 4. AKAP79-anchored PKA opposes CDI of $Ca_V1.2$ channels in tsA201 cells. Top, Superimposed Ca^{2+} (red) and Ba^{2+} (black) currents carried through $Ca_V1.2$ channels. Bottom, Inactivation rates for Ca^{2+} and Ba^{2+} currents. Currents were recorded during forskolin (FSK; 5 μM) activation of PKA, with overexpressed mutant AKAP79 lacking the CaN binding site (79ΔPIX) with no forskolin present, with a combination of 79ΔPIX and forskolin, or during PKI (5 μM) inhibition of PKA activity (no forskolin). *$p < 0.05$ (Student's t test); **$p < 0.001$ vs AKAP79 + wild-type $Ca_V1.2$ (by both ANOVA and Bonferroni's test). Control data for AKAP79-overexpressing cells, shown in gray, are reproduced from Figure 2*A* for comparison. Ca^{2+} current densities were as follows (in pA/pF): FSK, −25.7 ± 7.2; 79ΔPIX, −28.5 ± 4.7; 79ΔPIX + FSK, −30.1 ± 3.9; PKI, −25.5 ± 6.5.

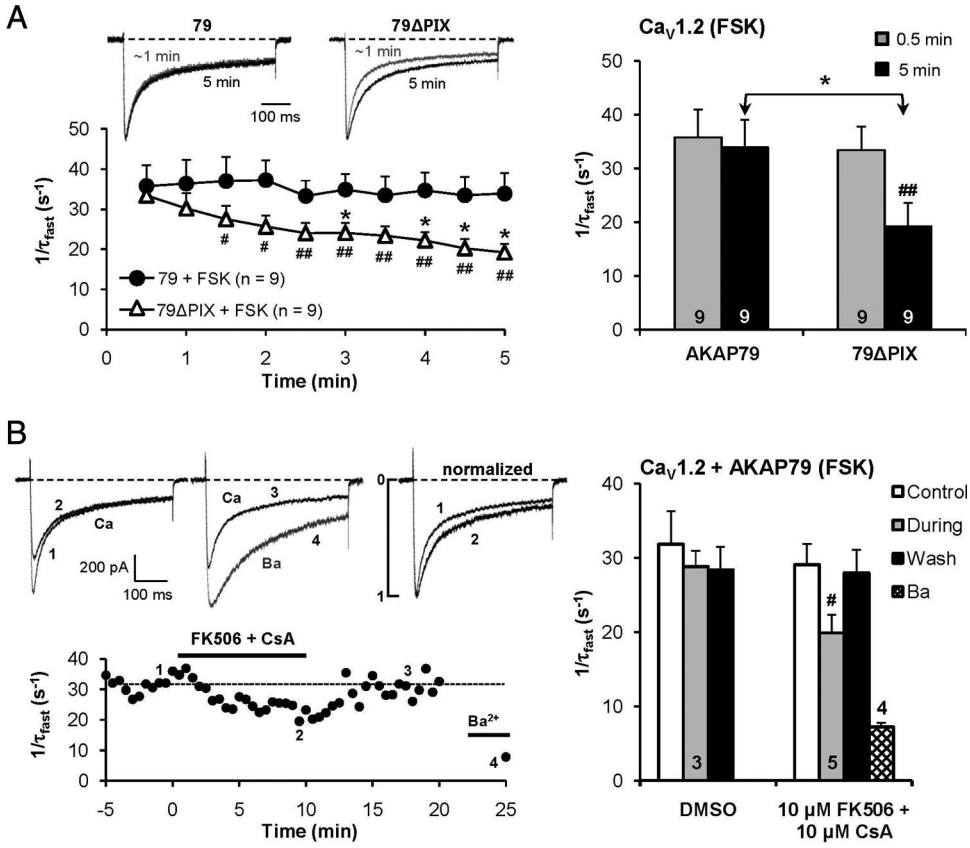

Figure 5. Time course of forskolin action supports a role for AKAP79-anchored calcineurin in CDI of $Ca_V1.2$ channels expressed in tsA201 cells. ***A***, Whole-cell recording with 5 μM forskolin in the pipette, with breakthrough into whole-cell mode at time 0 min. For cells transfected with 79ΔPIX, the rate of inactivation of Ca^{2+} current slowed as forskolin entered the cell. Cells transfected with wild-type AKAP79 (79) showed no slowing of CDI during intracellular perfusion with forskolin. #$p < 0.05$; ##$p < 0.01$ vs 0.5 min (paired t test); *$p < 0.05$ vs AKAP79. Ca^{2+} current densities were as follows (in pA/pF): 79 + FSK, −29.9 ± 5.6; 79ΔPIX + FSK, −25.0 ± 5.0. ***B***, Bath application of FK506 (10 μM) plus cyclosporin A (10 μM) significantly slowed inactivation of forskolin-enhanced $Ca_V1.2$ Ca^{2+} currents in cells overexpressing AKAP79. #$p < 0.05$ (paired t test). Top right, Ca^{2+} current records before and during drug application are scaled to the same peak amplitude to facilitate comparison of inactivation rate.

alternative models for the action of dephosphorylation in CDI. In a permissive model, dephosphorylation by CaN must precede downstream steps that carry out CDI, such as conformational rearrangement of Ca^{2+}/CaM on the C-terminal regulatory domains (PreIQ, IQ) of $Ca_V1.2$; dephosphorylation by CaN is a prerequisite for downstream steps to effectuate CDI. Alternatively, in a direct model of CaN's role in CDI, dephosphorylation is envisioned as the terminal regulatory step in CDI, and Ca^{2+}/CaM acts exclusively through CaN. In either case, the advantageous placement of CaN via anchoring on AKAP79/150 promotes CaN-dependent CDI. For highly abundant neuronal signaling molecules such as CaN (~1% of protein in brain neurons), AKAP-based scaffolding may not only serve to localize enzymes to their targets, but via steric protection may also help shield substrates from extraneous phosphorylation signaling. It remains to be determined whether these models or related ones apply in excitable cells other than hippocampal neurons. For either model of CaN action, a dephosphorylation-based mechanism of CDI adds to the richness of signaling mechanisms that regulate L-type Ca^{2+} channels in neurons.

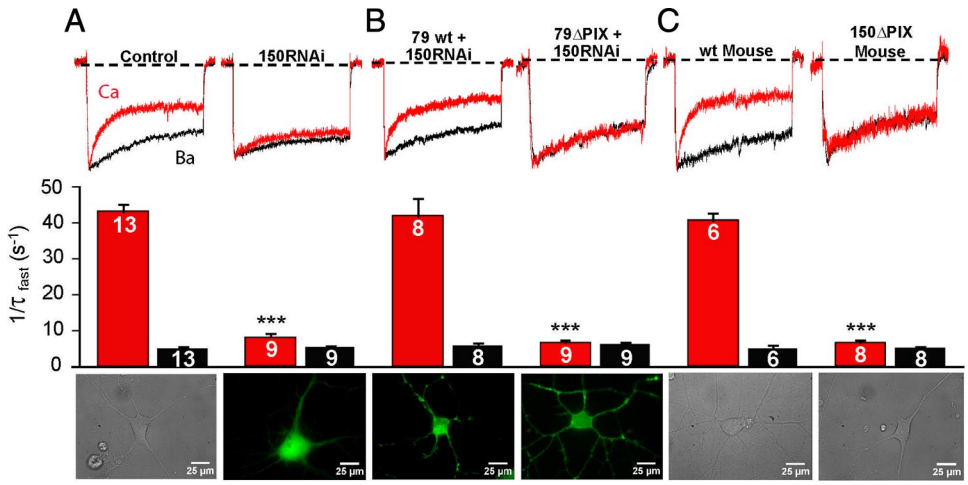

Figure 6. AKAP79/150-anchored CaN is required for CDI of L-type Ca^{2+} channels in dissociated, short-term cultured hippocampal neurons. ***A***, For rat neurons, pharmacologically isolated L channel Ca^{2+} (red) and Ba^{2+} (black) currents recorded from the same neuron, evoked by 500 ms depolarization from −60 to 0 mV. Peak Ca^{2+} current is normalized to peak Ba^{2+} current. Control neurons were transfected with GFP and the empty pSilencer vector. 150RNAi neurons were transfected with a short hairpin construct to suppress endogenous AKAP150 expression. Images of short-term cultured hippocampal neurons are a differential interference contrast (DIC) image of an untransfected hippocampal neuron (left) and a fluorescence image of hippocampal neuron expressing 150RNAi along with cytoplasmic GFP to mark transfected neurons (150RNAi; right). ***B***, Cultured rat neurons were transfected with 150RNAi and either AKAP79 [79 wild-type (wt); rescue] or *AKAP79ΔPIX* (79ΔPIX; failed rescue). Images of cultured neurons are a fluorescence image of a hippocampal neuron expressing 150RNAi and AKAP79 (left) and a fluorescence image of a rat cultured hippocampal neuron expressing 150RNAi and either AKAP79ΔPIX or AKAP150ΔPIX. ***C***, For mouse short-term cultured hippocampal neurons, pharmacologically isolated L channel Ca^{2+} (red) and Ba^{2+} (black) currents were recorded from the same neuron. DIC images of neurons from a wild-type mouse and a transgenic *AKAP150ΔPIX* mouse are shown. ***$p < 0.0001$ vs control (Student's *t* test). For inactivation rates, *n* values are indicated on the bars. Ca^{2+} current densities were as follows (in pA/pF): control, −32.2 ± 2.3; 150RNAi, −32.8 ± 2.0; 79 wt + 150RNAi, −29.2 ± 2.5; 79ΔPIX + 150RNAi, −28.7 ± 1.9; wt Mouse, −30.0 ± 2.1; 150ΔPIX Mouse, −31.9 ± 2.5.

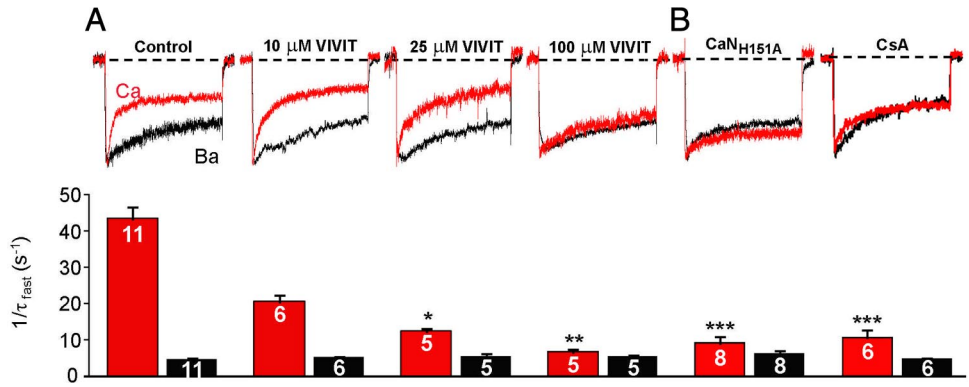

Figure 7. Acute inhibition of CaN anchoring and activity suppresses CDI in hippocampal neurons. ***A***, VIVIT peptide, a competitive inhibitor of CaN anchoring on AKAP150, dose-dependently suppresses CDI in dissociated, short-term cultured hippocampal neurons. VIVIT was perfused into neurons via the whole-cell patch pipette. Control neurons were recorded with 0.1% DMSO in the patch pipette, which was the concentration of DMSO in the VIVIT experiments. ***B***, Calcineurin phosphatase activity is required for Ca^{2+}-dependent inactivation of L-type channels in dissociated, short-term cultured hippocampal neurons. Top, Comparison of scaled currents evoked by 500 ms depolarization in Ca^{2+} versus Ba^{2+} for control, neurons transfected with CaN_{H151A}, and neurons internally perfused with cyclosporin A (5 μM). Bottom, Corresponding inactivation rates ($1/\tau_{fast}$). Control neurons were perfused with a whole-cell patch pipette solution containing 0.1% DMSO, which is the same concentration present in the cyclosporin A experiments. Results for CaN_{H151A} were compared to the control neurons in Figure 6 (no DMSO), while results with CsA were compared to the DMSO control. *$p = 0.01$; **$p < 0.005$; ***$p < 0.0001$ vs control neurons (Student's *t* test). Ca^{2+} current densities were as follows (in pA/pF): control, −31.3 ± 3.5; 10 μM VIVIT, −31.9 ± 5.0; 25 μM VIVIT, −31.5 ± 4.9; 100 μM VIVIT, −29.2 ± 4.0; CaN_{H151A}, −30.4 ± 2.2; and CsA, −32.6 ± 1.5.

Ser/Thr kinases that oppose CaN-dependent CDI

In hippocampal pyramidal neurons, β_2 adrenergic receptors are known to regulate L-type Ca^{2+} current through PKA (Gray and Johnston, 1987; Davare et al., 2001; Hoogland and Saggau, 2004), and in thalamocortical relay neurons, β_2 adrenergic receptor activation slows CDI (Rankovic et al., 2011). But β_2 adrenergic receptor activity is not the only potential means of activating PKA: a major adenylyl cyclase isotype in hippocampal pyramidal neurons is the Ca^{2+}-stimulable type 8, which is known to bind to AKAP79/150 (Willoughby et al., 2010). Thus, Ca^{2+} influx via L channels could locally stimulate adenylyl cyclase type 8 production of cAMP and hence PKA activity. Our results in cells expressing a CaN-anchoring-defective AKAPΔPIX construct, demonstrate that activation of PKA through forskolin stimulation of adenylyl cyclase reduced CDI, suggesting that phosphorylation by PKA opposes dephosphorylation by CaN. Inhibition of PKA by PKI also impacted CDI, but this treatment, too, slowed CDI. That both stimulation and inhibition of PKA slow CDI might be reconciled to some degree by the following: while PKA kinase activity reverses CaN phosphatase action and thus suppresses CDI, PKI inhibition of kinase activity may result in few channels remaining in a phosphorylated state and so few remain available to undergo CaN-dependent CDI. However, when compared to CaN inhibition, incomplete suppression of CDI by PKI suggests contributions from other signaling processes.

CDF of L channels is also a phosphosignaling-based process and one that overlaps CDI, as CDF can be detected as a reduction in CDI (Wu et al., 2001; Hudmon et al., 2005; Erxleben et al., 2006; Grueter

et al., 2006). CDF is mediated by channel-associated Ca^{2+}/CaMKII activity, which is not only congruent with a phosphatase-based mechanism for CDI, but also indicates that kinases other than PKA may be involved in CDI. Indeed, because our experiments showed that a high concentration of PKI was unable to prevent CDI entirely, as predicted if PKA were solely responsible for recovery from CaN-dependent inactivation, it seems likely that additional kinases may contribute to phosphorylation of the CaN-sensitive CDI substrate. CaMKII is one likely candidate, as it associates with $Ca_V1.2$ channels and enhances their activity. If CaMKII cooperates with PKA to oppose CaN action, it is intriguing to consider how Ca^{2+}/CaM molecules residing in the channel's nanodomain are able to initiate signaling to CaMKII or CaN and thereby initiate either CaMKII-dependent facilitation or CaN-dependent inactivation (Saucerman and Bers, 2008).

Previous evidence for CaN-dependent CDI

Considering that an enzymatic mechanism for CDI of Ca_V channels was proposed over two decades ago (Chad and Eckert, 1986; for review, see Armstrong, 1989), why has a role for CaN in CDI fallen into disfavor? One likely reason is that channel-associated CaN activity is difficult to suppress. CsA and FK506 are the most commonly used CaN inhibitors, but CsA and FK506 were much less effective in preventing CDI when compared to the CaN AIP (Figs. 2*C*, 5*B*). This may be related to the mechanism of action of CsA and FK506, which must first bind to immunophilins and then inhibit CaN activity as drug-immunophilin complexes. Because such complexes are much larger (>18 kDa) than the CaN AIP (a 25-mer polypeptide of 2.9 kDa), it is possible that CaN may be protected from inhibition by drug-immunophilin complexes when the phosphatase is tightly associated with the channel. In some cases, the effectiveness of CaN-inhibiting drugs like CsA has also been found to be limited by immunophilin expression level (Kung and Halloran, 2000; Mitchell et al., 2002). In our experiments in tsA201 cells, CaN_{H151A} expression did not fully suppress CDI unless AKAP79/150 targeting of CaN was also disrupted, indicating that CaN-dependent channel inactivation is more resistant to perturbation when CaN is scaffolded to the channel. Although AKAP79/150 is expressed in every cell type where $Ca_V1.2$ is found and in most heterologous expression systems used to study $Ca_V1.2$ channels, including HEK293 and tsA201cells, the level of AKAP79/150 expression varies widely between cell types and might therefore explain partial or conflicting effects of CaN inhibitors on CDI.

Another confounding factor arises from the reliance upon Ba^{2+} to isolate CDI. But Ba^{2+} weakly supports CDI (Fig. 3), making it more challenging to work out the molecular mechanism of this process. Many divalent cations are able to activate CaM, their effectiveness as substitutes for Ca^{2+} largely depending on how closely they approximate Ca^{2+} in ionic radius (Chao et al., 1984). The difference in size between Ba^{2+} and Ca^{2+} generally makes Ba^{2+} a poor substitute for Ca^{2+}, but several factors may facilitate Ba^{2+} binding to CaM within the channel complex: (1) $[Ba^{2+}]$, like $[Ca^{2+}]$, reaches high levels in the nanodomain near the channel mouth, (2) Ba^{2+} is poorly chelated by EGTA or BAPTA, and (3) Ba^{2+} is slowly sequestered by cellular transporters. Ba^{2+} has been found to activate other Ca^{2+}-sensitive processes including neurotransmitter release (McMahon and Nicholls, 1993), Ca^{2+} release from internal stores (Satoh et al., 1987), contraction of skeletal (Stephenson and Thieleczek, 1986) and smooth muscle (Satoh et al., 1987), gene expression (Curran and Morgan, 1986), and cAMP production by Ca^{2+}-sensitive adenylyl cyclases (Gu and Cooper, 2000).

Conclusions

In cultured hippocampal pyramidal neurons, CaN and PKA appear to work by opposing mechanisms of CDI/de-enhancement versus enhancement. Because multiple phosphorylation sites may be involved, and other kinases such as CaMKII or phosphatases such as PP2A (Xu et al., 2010), CaN versus PKA expressed as CDI versus enhancement may prove to be an oversimplification. The AKAP79/150 PxIxIT-like motif and $Ca_V1.2$ IQ motif play supporting roles in positioning CaN and CaM near the source of Ca^{2+}, but preassembly of CaM with CaN may also help speed enzymatic CDI. The affinity of AKAP79/150 for CaN is relatively low ($K_D \approx 0.5\ \mu M$), perhaps anchoring CaN just tightly enough to target it in cells while also permitting sufficiently rapid release from the AKAP to promote regulation of nearby substrates (Li et al., 2012).

References

Adams B, Tanabe T (1997) Structural regions of the cardiac Ca channel α_{1C} subunit involved in Ca-dependent inactivation. J Gen Physiol 110:379–389. CrossRef Medline

Alseikhan BA, DeMaria CD, Colecraft HM, Yue DT (2002) Engineered calmodulins reveal the unexpected eminence of Ca^{2+} channel inactivation in controlling heart excitation. Proc Natl Acad Sci U S A 99:17185–17190. CrossRef Medline

Armstrong DL (1989) Calcium channel regulation by calcineurin, a Ca^{2+}-activated phosphatase in mammalian brain. Trends Neurosci 12:117–122. CrossRef Medline

Bean BP, Nowycky MC, Tsien RW (1984) β-Adrenergic modulation of calcium channels in frog ventricular heart cells. Nature 307:371–375. CrossRef Medline

Branchaw JL, Banks MI, Jackson MB (1997) Ca^{2+}- and voltage-dependent inactivation of Ca^{2+} channels in nerve terminals of the neurohypophysis. J Neurosci 17:5772–5781. Medline

Brehm P, Eckert R (1978) Calcium entry leads to inactivation of calcium channel in *Paramecium*. Science 202:1203–1206. CrossRef Medline

Burley JR, Sihra TS (2000) A modulatory role for protein phosphatase 2B (calcineurin) in the regulation of Ca^{2+} entry. Eur J Neurosci 12:2881–2891. CrossRef Medline

Calin-Jageman I, Lee A (2008) Ca_V1 L-type Ca^{2+} channel signaling complexes in neurons. J Neurochem 105:573–583. CrossRef Medline

Chad JE, Eckert R (1986) An enzymatic mechanism for calcium current inactivation in dialysed Helix neurones. J Physiol 378:31–51. Medline

Chao SH, Suzuki Y, Zysk JR, Cheung WY (1984) Activation of calmodulin by various metal cations as a function of ionic radius. Mol Pharmacol 26:75–82. Medline

Curran T, Morgan JI (1986) Barium modulates c-fos expression and post-translational modification. Proc Natl Acad Sci U S A 83:8521–8524. CrossRef Medline

Davare MA, Avdonin V, Hall DD, Peden EM, Burette A, Weinberg RJ, Horne MC, Hoshi T, Hell JW (2001) A β_2 adrenergic receptor signaling complex assembled with the Ca^{2+} channel $Ca_V1.2$. Science 293:98–101. CrossRef Medline

Dolmetsch RE, Pajvani U, Fife K, Spotts JM, Greenberg ME (2001) Signaling to the nucleus by an L-type calcium channel-calmodulin complex through the MAP kinase pathway. Science 294:333–339. CrossRef Medline

Erickson MG, Alseikhan BA, Peterson BZ, Yue DT (2001) Preassociation of calmodulin with voltage-gated Ca^{2+} channels revealed by FRET in single living cells. Neuron 31:973–985. CrossRef Medline

Erickson MG, Liang H, Mori MX, Yue DT (2003) FRET two-hybrid mapping reveals function and location of L-type Ca^{2+} channel CaM preassociation. Neuron 39:97–107. CrossRef Medline

Erxleben C, Liao Y, Gentile S, Chin D, Gomez-Alegria C, Mori Y, Birnbaumer L, Armstrong DL (2006) Cyclosporin and Timothy syndrome increase mode 2 gating of $Ca_V1.2$ calcium channels through aberrant phosphorylation of S6 helices. Proc Natl Acad Sci U S A 103:3932–3937. CrossRef Medline

Gomez LL, Alam S, Smith KE, Horne E, Dell'Acqua ML (2002) Regulation of A-kinase anchoring protein 79/150-cAMP-dependent protein kinase postsynaptic targeting by NMDA receptor activation of calcineurin and remodeling of dendritic actin. J Neurosci 22:7027–7044. Medline

Gordon GW, Berry G, Liang XH, Levine B, Herman B (1998) Quantitative fluorescence resonance energy transfer measurements using fluorescence microscopy. Biophys J 74:2702–2713. CrossRef Medline

Gray R, Johnston D (1987) Noradrenaline and β-adrenoceptor agonists increase activity of voltage-dependent calcium channels in hippocampal neurons. Nature 327:620–622. CrossRef Medline

Grueter CE, Abiria SA, Dzhura I, Wu Y, Ham AJ, Mohler PJ, Anderson ME, Colbran RJ (2006) L-type Ca^{2+} channel facilitation mediated by phosphorylation of the beta subunit by CaMKII. Mol Cell 23:641–650. CrossRef Medline

Gu C, Cooper DM (2000) Ca^{2+}, Sr^{2+}, and Ba^{2+} identify distinct regulatory sites on adenylyl cyclase (AC) types VI and VIII and consolidate the apposition of capacitative cation entry channels and Ca^{2+}-sensitive ACs. J Biol Chem 275:6980–6986. CrossRef Medline

Hadley RW, Lederer WJ (1991) Ca^{2+} and voltage inactivate Ca^{2+} channels in guinea-pig ventricular myocytes through independent mechanisms. J Physiol 444:257–268. Medline

Hoogland TM, Saggau P (2004) Facilitation of L-type Ca^{2+} channels in dendritic spines by activation of β_2 adrenergic receptors. J Neurosci 24:8416–8427. CrossRef Medline

Hoshi N, Langeberg LK, Scott JD (2005) Distinct enzyme combinations in AKAP signalling complexes permit functional diversity. Nat Cell Biol 7:1066–1073. CrossRef Medline

Hudmon A, Schulman H, Kim J, Maltez JM, Tsien RW, Pitt GS (2005) CaMKII tethers to L-type Ca^{2+} channels, establishing a local and dedicated integrator of Ca^{2+} signals for facilitation. J Cell Biol 171:537–547. CrossRef Medline

Kalman D, O'Lague PH, Erxleben C, Armstrong DL (1988) Calcium-dependent inactivation of the dihydropyridine-sensitive calcium channels in GH3 cells. J Gen Physiol 92:531–548. CrossRef Medline

Kim J, Ghosh S, Nunziato DA, Pitt GS (2004) Identification of the components controlling inactivation of voltage-gated Ca^{2+} channels. Neuron 41:745–754. CrossRef Medline

Kung L, Halloran PF (2000) Immunophilins may limit calcineurin inhibition by cyclosporine and tacrolimus at high drug concentrations. Transplantation 70:327–335. CrossRef Medline

Lee KS, Marban E, Tsien RW (1985) Inactivation of calcium channels in mammalian heart cells: joint dependence on membrane potential and intracellular calcium. J Physiol 364:395–411. Medline

Li H, Pink MD, Murphy JG, Stein A, Dell'Acqua ML, Hogan PG (2012) Balanced interactions of calcineurin with AKAP79 regulate Ca^{2+}-calcineurin-NFAT signaling. Nat Struct Mol Biol 19:337–345. CrossRef Medline

Lukyanetz EA, Piper TP, Sihra TS (1998) Calcineurin involvement in the regulation of high-threshold Ca^{2+} channels in NG108–15 (rodent neuroblastoma x glioma hybrid) cells. J Physiol 510:371–385. CrossRef Medline

McCleskey EW, Fox AP, Feldman DH, Cruz LJ, Olivera BM, Tsien RW, Yoshikami D (1987) ω-Conotoxin: direct and persistent blockade of specific types of calcium channels in neurons but not muscle. Proc Natl Acad Sci U S A 84:4327–4331. CrossRef Medline

McMahon HT, Nicholls DG (1993) Barium-evoked glutamate release from guinea-pig cerebrocortical synaptosomes. J Neurochem 61:110–115. CrossRef Medline

Meuth S, Pape HC, Budde T (2002) Modulation of Ca^{2+} currents in rat thalamocortical relay neurons by activity and phosphorylation. Eur J Neurosci 15:1603–1614. CrossRef Medline

Mitchell PO, Mills ST, Pavlath GK (2002) Calcineurin differentially regulates maintenance and growth of phenotypically distinct muscles. Am J Cell Physiol 282:C984–C992. Medline

Mochida S, Few AP, Scheuer T, Catterall WA (2008) Regulation of presynaptic $Ca_V2.1$ channels by Ca^{2+} sensor proteins mediates short-term synaptic plasticity. Neuron 57:210–216. CrossRef Medline

Mondragon A, Griffith EC, Sun L, Xiong F, Armstrong C, Liu JO (1997) Overexpression and purification of human calcineurin alpha from Escherichia coli and assessment of catalytic functions of residues surrounding the binuclear metal center. Biochemistry 36:4934–4942. CrossRef Medline

Noble S, Shimoni Y (1981) The calcium and frequency dependence of the slow inward current 'staircase' in frog atrium. J Physiol 310:57–75. Medline

Oliveria SF, Dell'Acqua ML, Sather WA (2007) AKAP79/150 anchoring of calcineurin controls neuronal L-type Ca^{2+} channel activity and nuclear signaling. Neuron 55:261–275. CrossRef Medline

Peterson BZ, DeMaria CD, Adelman JP, Yue DT (1999) Calmodulin is the Ca^{2+} sensor for Ca^{2+}-dependent inactivation of L-type calcium channels. Neuron 22:549–558. CrossRef Medline

Pitt GS, Zühlke RD, Hudmon A, Schulman H, Reuter H, Tsien RW (2001) Molecular basis of calmodulin tethering and Ca^{2+}-dependent inactivation of L-type Ca^{2+} channels. J Biol Chem 276:30794–30802. CrossRef Medline

Rankovic V, Landgraf P, Kanyshkova T, Ehling P, Meuth SG, Kreutz MR, Budde T, Munsch T (2011) Modulation of calcium-dependent inactivation of L-type Ca^{2+} channels via β-adrenergic signaling in thalamocortical relay neurons. PLoS One 6:e27474. CrossRef Medline

Sanderson JL, Gorski JA, Gibson ES, Lam P, Freund RK, Chick WS, Dell'Acqua ML (2012) AKAP150-anchored calcineurin regulates synaptic plasticity by limiting synaptic incorporation of Ca^{2+}-permeable AMPA receptors. J Neurosci, in press.

Sather WA, Tanabe T, Zhang JF, Mori Y, Adams ME, Tsien RW (1993) Distinctive biophysical and pharmacological properties of class A (BI) calcium channel α_1 subunits. Neuron 11:291–303. CrossRef Medline

Satoh S, Kubota Y, Itoh T, Kuriyama H (1987) Mechanisms of the Ba^{2+}-induced contraction in smooth muscle cells of the rabbit mesenteric artery. J Gen Physiol 89:215–237. CrossRef Medline

Saucerman JJ, Bers DM (2008) Calmodulin mediates differential sensitivity of CaMKII and calcineurin to local Ca^{2+} in cardiac myocytes. Biophys J 95:4597–4612. CrossRef Medline

Smith KE, Gibson ES, Dell'Acqua ML (2006) cAMP-dependent protein kinase postsynaptic localization regulated by NMDA receptor activation through translocation of an A-kinase anchoring protein scaffold protein. J Neurosci 26:2391–2402. CrossRef Medline

Sochivko D, Chen J, Becker A, Beck H (2003) Blocker-resistant Ca^{2+} currents in rat CA1 hippocampal pyramidal neurons. Neuroscience 116:629–638. CrossRef Medline

Stephenson DG, Thieleczek R (1986) Activation of the contractile apparatus of skinned fibres of frog by the divalent cations barium, cadmium and nickel. J Physiol 380:75–92. Medline

Tavalin SJ, Shepherd D, Cloues RK, Bowden SE, Marrion NV (2004) Modulation of single channels underlying hippocampal L-type current enhancement by agonists depends on the permeant ion. J Neurophysiol 92:824–837. CrossRef Medline

Victor RG, Rusnak F, Sikkink R, Marban E, O'Rourke B (1997) Mechanism of Ca^{2+}-dependent inactivation of L-type Ca^{2+} channels in GH3 cells: direct evidence against dephosphorylation by calcineurin. J Membr Biol 156:53–61. CrossRef Medline

Willoughby D, Masada N, Wachten S, Pagano M, Halls ML, Everett KL, Ciruela A, Cooper DM (2010) AKAP79/150 interacts with AC8 and regulates Ca^{2+}-dependent cAMP synthesis in pancreatic and neuronal systems. J Biol Chem 285:20328–20342. CrossRef Medline

Wu Y, Dzhura I, Colbran RJ, Anderson ME (2001) Calmodulin kinase and a calmodulin-binding 'IQ' domain facilitate L-type Ca^{2+} current in rabbit ventricular myocytes by a common mechanism. J Physiol 535:679–687. CrossRef Medline

Xu H, Ginsburg KS, Hall DD, Zimmermann M, Stein IS, Zhang M, Tandan S, Hill JA, Horne MC, Bers D, Hell JW (2010) Targeting of protein phosphatases PP2A and PP2B to the C-terminus of the L-type calcium channel $Ca_V1.2$. Biochemistry 49:10298–10307. CrossRef Medline

Zeilhofer HU, Blank NM, Neuhuber WL, Swandulla D (2000) Calcium-dependent inactivation of neuronal calcium channel currents is independent of calcineurin. Neuroscience 95:235–241. Medline

Zühlke RD, Pitt GS, Deisseroth K, Tsien RW, Reuter H (1999) Calmodulin supports both inactivation and facilitation of L-type calcium channels. Nature 399:159–162. CrossRef Medline

Zühlke RD, Pitt GS, Tsien RW, Reuter H (2000) Ca^{2+}-sensitive inactivation and facilitation of L-type Ca^{2+} channels both depend on specific amino acid residues in a consensus calmodulin binding motif in the alpha 1C subunit. J Biol Chem 275:21121–21129. CrossRef Medline